ACS Medicinal Chemistry Letters

pubs.acs.org/acsmedchemlett
Letter

Design, Synthesis, and Evaluation of a New Fluorescent Ligand for the M_2 Muscarinic Acetylcholine Receptor

Renáta Szabó, Dénes Szepesi Kovács, Dóra Judit Kiss, Zeinab Nezafat Yazdi, András Dávid Tóth, Jose Brea, María Isabel Loza, Domokos Meszéna, Lucia Wittner, István Ulbert, Balázs Volk, László Hunyady, and György Miklós Keserű*

Cite This: ACS Med. Chem. Lett. 2025, 16, 552−559

Read Online

ACCESS | Metrics & More | Article Recommendations | Supporting Information

ABSTRACT: The M_2 muscarinic acetylcholine receptor (M_2R) is a G protein-coupled receptor involved in regulating cardiovascular functions and mediation of central muscarinic effects, such as movement, temperature control, and antinociceptive responses. Molecular probes targeting this receptor are therefore important in exploring its pathophysiological role at a molecular level. Herein, we report the design, synthesis, and evaluation of a new fluorescent probe for M_2R based on an anthranilamide ligand. In radioligand binding experiments, the presented Oregon Green 488-labeled conjugate (**33**) exhibited high M_2R affinity (K_i = 2.4 nM), a moderate preference for the M_2R over the M_4 receptor, and excellent to pronounced M_2R selectivity compared to the M_1, M_3, and M_5 receptors. The utility of the probe was demonstrated in confocal, two-photon, and stimulated emission depletion nanoscopy (STED) imaging to specifically label the receptors in human embryonic kidney (HEK) 293T cells. These properties suggest that our probe may be utilized in advanced microscopy to study the pharmacology of the M_2R.

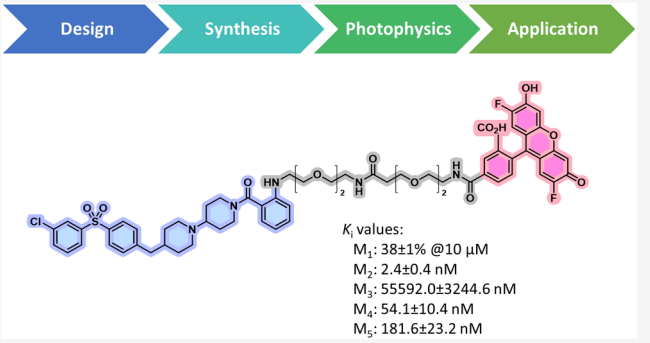

KEYWORDS: *fluorescent probe, G protein-coupled receptor, imaging, two-photon microscopy, STED nanoscopy*

Muscarinic acetylcholine receptors (mAChRs) are G protein-coupled receptors (GPCRs) with five subtypes (M_1−M_5) divided into two functional classes based on G protein coupling: M_1, M_3, and M_5 with G_q and M_2 and M_4 with G_i/G_o.[1] Activation of mAChRs by agonists like acetylcholine (ACh) triggers biochemical and electrophysiological responses, depending on the receptor subtype and location. Involved in both central and parasympathetic nervous systems,[2] muscarinic receptors are therapeutic targets for conditions like Alzheimer's disease (AD), addiction, epilepsy, schizophrenia, and Parkinson's disease.[3−5]

Designing subtype-selective mAChR ligands remains a significant challenge for medicinal chemists. Early efforts focused on compounds with a pyridobenzodiazepinone core (**1**, **2**), but their selectivity versus other muscarinic receptor subtypes is modest (Figure 1).[6,7] The discovery of potent M_2R antagonists led to the synthesis of piperidine analogues, including **3**, a highly potent and selective antagonist with poor pharmacokinetics.[5,8] Further optimization focused on reducing clearance rates and enhancing selectivity, leading to antagonist **4**, which replaces the (2-methyl)benzoyl group of **3** with an anthranilic acid amide. This compound (**4**) shows high M_2R selectivity, good oral bioavailability, and *in vivo* efficacy in rats.[9]

Various fluorescent probes for muscarinic receptors prepared by the conjugation of a ligand with a fluorophore have been reported in the literature. These fluorescent ligands are based on derivatives preferring the M_1 subtype, e.g., pirenzepine,[10−12] telenzepine,[13,14,12] and AC-42,[15] and those preferring the M_3 subtype, e.g., tolterodine.[16] Few studies used ligands (structurally closely related to pyridobenzodiazepinones shown in Figure 1) with various fluorescent dyes having high affinity but moderate selectivity for M_2R (Figure 2). These probes exhibit potential for use in imaging and binding studies with evidence suggesting a dualsteric mode of action.[17−20] Unfortunately, despite all efforts, these fluorescent M_2R ligands lack selectivity toward the M_1 and M_4 receptors.[21]

In recent years, modern high-resolution imaging techniques have become useful and common tools for visualization and dynamic monitoring.[22] Confocal microscopy is a widely used

Received: December 7, 2024
Revised: February 28, 2025
Accepted: March 13, 2025
Published: March 20, 2025

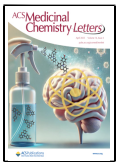

https://doi.org/10.1021/acsmedchemlett.4c00592
ACS Med. Chem. Lett. 2025, 16, 552−559

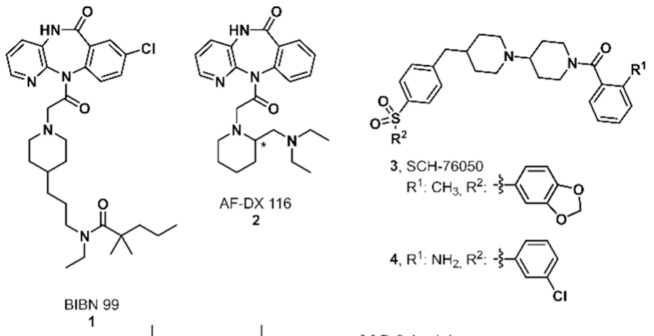

Compound	M_2R K_i [nM]	M_2R Selectivity over M_1, M_3, M_4, M_5 Subtypes			
		M_1/M_2	M_3/M_2	M_4/M_2	M_5/M_2
1	30.2	35	26	6	48
2	105.0	7	16	4	44
3	0.02	1400	730	37	280
4	0.20	2926	2722	148	186

Figure 1. Structural formulas, M_2R affinities, and M_2R selectivity over M_1, M_3, M_4, and M_5 subtypes of M_2R antagonists.[6−9]

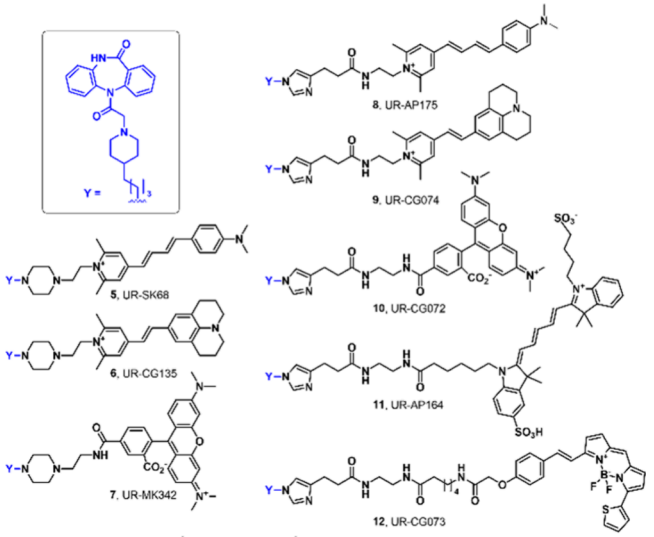

Compound	M_2R K_i [nM]	M_2R Selectivity over M_1, M_3, M_4, M_5 Subtypes			
		M_1/M_2	M_3/M_2	M_4/M_2	M_5/M_2
5	3.2	4.0	50.1	3.2	125.9
6	1.0	5.0	66.0	2.8	131.8
7	0.2	10.7	338.8	4.1	741.3
8	0.9	5.4	93.3	4.7	77.6
9	1.3	5.2	51.3	1.9	30.1
10	1.7	3.4	72.4	2.0	154.8
11	0.8	6.3	199.5	39.8	199.5
12	0.7	1.4	53.7	0.6	14.5

Figure 2. Structures, M_2R binding data, and M_2R selectivity over M_1, M_3, M_4, and M_5 subtypes of dibenzodiazepinone-type fluorescent ligands conjugated with various fluorescent dyes reported in the literature.[17,20]

technique for studying the labeling of proteins with fluorescent probes[23−27] while there are a number of examples of two-photon microscopy[28,29] and stimulated emission depletion nanoscopy (STED) reported in the literature.[30−32] Two-photon and STED imaging techniques offer efficient visualization with significant advantages over confocal microscopy for three-dimensional fluorescence imaging.[32] These benefits include enhanced 3D resolution and a minimized photodamage.

In the present study, we report a new fluorescently labeled anthranilamide-type M_2R ligand using Oregon Green 488 (OG488) fluorescent dye to improve the selectivity and to broaden the scope of the application compared to existing probes. The OG488 fluorophore was chosen because it has a high extinction coefficient and fluorescence quantum yield, and it is suitable for both two-photon microscopy and STED imaging.

Results and Discussion. While searching for selective M_2 antagonists in the literature, we selected compound **4**.[9] Based on the published data obtained by radioligand displacement assays, **4** shows high affinity (K_i = 0.2 nM) on the M_2 receptor and exhibits remarkable selectivity toward most muscarinic receptor subtypes with values of 2926, 2722, 148, and 186 against M_1, M_3, M_4, and M_5, respectively (Figure 1). As the experimental binding mode of this compound is unknown, computational tools have been used to predict its binding pose and to design the appropriate attachment point and length of the linker. For these structure-based calculations, we started from the crystal structure of the receptor available in the Protein Data Bank (PDB: 5ZKB).[33] As our selected ligand core differs from the ligand in the experimental structure, induced fit docking calculations have been run that allow the movement and adaptation of the side chains in the binding site in order to determine the binding mode of the ligand (Figure 3). Several plausible binding poses have been obtained;

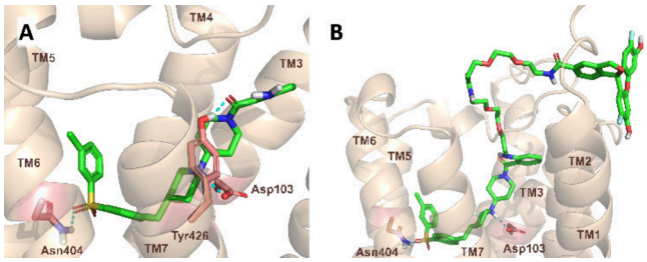

Figure 3. Design of the fluorescent probe. (A) The predicted binding mode of the base compound (**28**) and (B) the fluorescently labeled molecule (**33**). The receptor is represented as a wheat cartoon and the ligand, as green licorice; the hydrogen bonds are indicated with cyan dashed lines.

therefore, we have further assessed their stability with binding pose metadynamics. In the most plausible binding mode (Figure 3a), the ligand is stabilized in a dualsteric binding mode occupying the orthosteric pocket and also extending toward the extracellular vestibule interacting with residues on the top part of TM2,3,7 and ECL2. The molecule is anchored to the conserved Asp103$^{3.32}$ by a hydrogen bond and further stabilized with two additional hydrogen bonds with Asn404$^{6.52}$ and Tyr426$^{7.39}$. Linker attachment on the free amine group was chosen as the best exit vector since it is positioned toward the extracellular side and allows the elongation of the ligand without installing additional substituents into the core. Docking calculations into the grid prepared based on the ligand-bound structure obtained from IFD showed that two PEG_3 linkers positioned the attachment of the Oregon Green

https://doi.org/10.1021/acsmedchemlett.4c00592
ACS Med. Chem. Lett. 2025, 16, 552−559

488 dye well outside the extracellular side of the receptor, therefore allowing the ligand core of the conjugate to occupy the same binding pose as the original small ligand.

Based on the information obtained from the molecular docking studies, a novel fluorescent antagonist for the M_2 receptor was synthesized featuring an OG488-based probe. The synthetic route to the desired probe is illustrated in Schemes 1−3.

Scheme 1. Synthesis of the Sulfone Core[a]

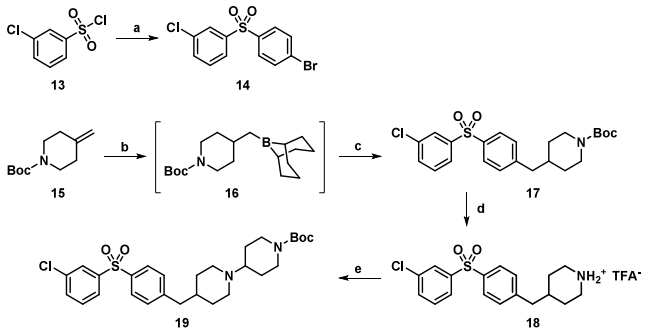

[a]Reagents and conditions: (a) bromobenzene, $AlCl_3$, 80 °C, 1 h, 81%; (b) 9-BBN, 65 °C, 1 h; (c) **14**, $PdCl_2(dppf)\cdot CH_2Cl_2$, K_2CO_3, DMF:water (10:1), 60 °C, 3 h, 83%; (d) TFA, DCM, 25 °C, 2 h, 93%; (e) 1-Boc-4-bromopiperidine, K_2CO_3, KI, MeCN, 80 °C, 24 h, 78%.

For the first step, we developed an efficient solvent- and chromatography-free synthesis of sulfone **14** (Scheme 1). We have found that bromobenzene could be acylated with 3-chlorobenzenesulfonyl chloride (**13**) in the presence of aluminum chloride ($AlCl_3$) at 80 °C to afford the expected sulfone (**14**) in excellent yield. Then, we followed the literature procedure[9] for the synthesis of intermediate **17**. Boc-protected methylidene piperidine **15** was treated with 9-BBN to form a borane intermediate (**16**), which was then coupled with bromoarylsulfone **14** in the presence of a palladium catalyst to produce compound **17**. The Boc group was removed, and the corresponding amine was generated as its TFA salt (**18**). Then, N-alkylation with 1-Boc-4-bromopiperidine followed to give **19**.

Subsequently, compound **25** was prepared using the available literature protocols (Scheme 2).[34,35] The synthesis of the final intermediates containing the PEG functionalized tail was started by selective protection of one amino group of commercially available **22** with Boc_2O in DCM. The resulting Boc-protected amine was coupled with 2-iodobenzoic acid under copper catalysis at room temperature to give **23**. The next step was the removal of the Boc functional group under acidic conditions to generate the corresponding amine as its TFA salt (**24**). The carboxylic acid group of compound **20** was activated with *N*-hydroxysuccinimide to afford **21**. Then, the amine (**24**) was N-acylated with NHS-ester-activated compound (**21**) to give compound **25**.

The Boc group in **19** was removed, and the resulting piperidine (**26**) was coupled with various carboxylic acids (Boc-2-Abz-OH, **23**, **25**) under standard conditions (Scheme 3). The Boc protecting group was then removed, and three different amine intermediates were obtained (**28**, **30**, **32**). Finally, **32** was coupled to the appropriate commercially available OG488 succinimidyl esters. The novel fluorescent conjugate **33** was isolated and purified by preparative HPLC.

Scheme 2. Synthesis of the PEG Linker Containing Derivatives[a]

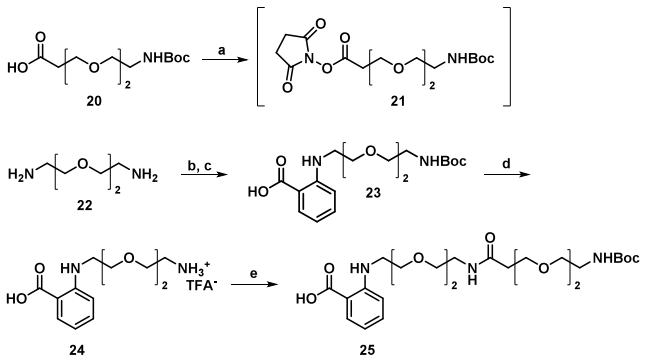

[a]Reagents and conditions: (a) NHS, DCC, THF, 25 °C, 2 h; (b) Boc_2O, DCM, 0 °C → 25 °C, 24 h; (c) 2-iodobenzoic acid, CuI, rac-BINOL, K_3PO_4, DMF, 25 °C, 3 h, 69%; (d) TFA, DCM, 25 °C, 2 h, 93%; (e) **21**, TEA, 25 °C, 0.5 h, 60%.

Scheme 3. Synthesis of the PEG-Containing Intermediates and the Novel Fluorescent M_2R Antagonist 33[a]

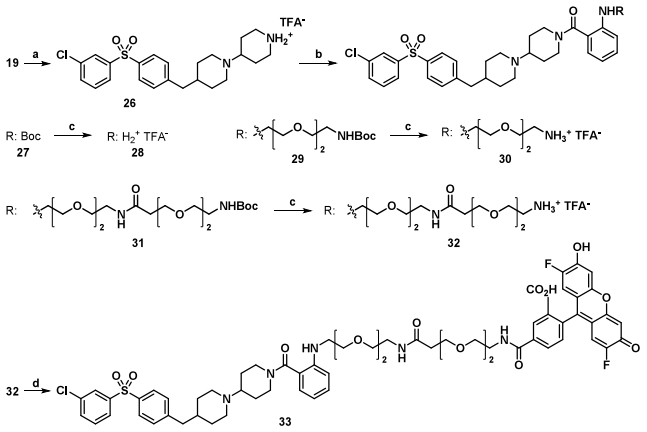

[a]Reagents and conditions: (a) TFA, DCM, 25 °C, 2 h, 95%; (b) Boc-2-Abz-OH or **23** or **25**, $HOBt\cdot H_2O$, EDC·HCl, TEA, DMF, 25 °C, 2 h, 55% (**27**); 50% (**29**); 48% (**31**); (c) TFA, DCM, 25 °C, 2 h, 95% (**28**); 92% (**30**); 97% (**32**); (d) OG488-NHS, DIPEA, DMF, 25 °C, 0.5 h, 40%.

Additionally, the chemical identity of new compounds and that of the probe was confirmed by NMR and high-resolution mass spectrometry (HRMS).

Next, we investigated the photophysical properties of the fluorescent probe **33**. In acetonitrile, the probe has an absorption maximum at 520 nm and a fluorescence maximum at 547 nm with a Stokes shift of 27 nm. The molar extinction coefficient (ε = 42504.9 M^{-1} cm^{-1}), fluorescence quantum yield (Φ_f = 0.20), and brightness (f = 8501) values are lower than those of the original dye[36] but are considered adequate for future biological applications. Figure S1 shows the absorbance and fluorescence spectra of probe **33** in various solvents, including DCM, dioxane, ethanol, ethyl acetate, phosphate buffered saline (PBS), THF, toluene, water, and acetonitrile. Higher solvent polarity correlated with increased fluorescence intensity, while aqueous media showed a lower intensity. The dye was pH sensitive, with intensity increasing at higher pH. Following a literature procedure, we examined the effect of protein (BSA) on the ligand.[20] We found that the

https://doi.org/10.1021/acsmedchemlett.4c00592
ACS Med. Chem. Lett. 2025, 16, 552−559

Table 1. Results of Binding Affinity of Compounds 28, 30, 32, and 33 Tested[a]

Compounds	Receptor K_i [nM]				
	M_1	M_2	M_3	M_4	M_5
28	425 ± 32	1.1 ± 0.2	193 ± 23	9.4 ± 1.1	119.0 ± 20.0
30	143 ± 11	1.5 ± 0.3	496 ± 36	7.4 ± 0.6	8.6 ± 0.7
32	113 ± 8	1.1 ± 0.1	373 ± 38	6.2 ± 0.9	8.5 ± 0.9
33	n.d.[b]	2.4 ± 0.4	55592 ± 3245	54.1 ± 10.4	182 ± 23

[a]Results are the mean ± SD of three independent experiments (n = 3). [b]K_i value could not be determined because inhibition at 10 μM was only 38 ± 1%.

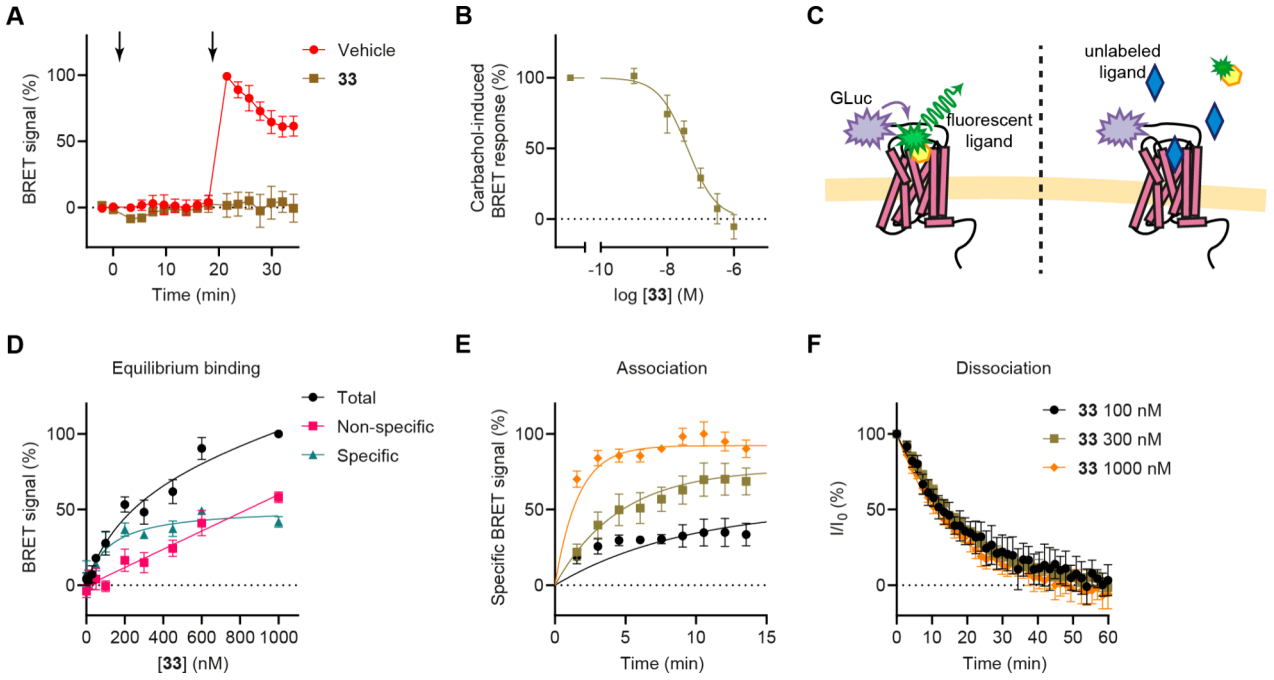

Figure 4. Functional activity and BRET-based ligand binding results. (A) Kinetic measurement of M_2R activity in the TRUPATH G_{oA} assay. The first arrow indicates the time of treatment with either vehicle or 300 nM compound **33**, while the second arrow marks the application of 10 μM carbachol. (B) Concentration−response analysis of the antagonistic effect of compound **33** on 10 μM carbachol-induced G_{oA} activation in the TRUPATH assay, and the IC_{50} value is shown in Table 2. (C) Schematic representation of the BRET-based ligand binding assay. (D) Equilibrium BRET-based ligand binding data. Nonspecific signals were determined using a 5 min pretreatment with 100 μM atropine. (E) Kinetic measurement of **33** binding to assess association kinetics. Data from a representative measurement performed in triplicate are shown and represented as mean ± SD. The experiment was repeated three times with consistent results. The "Association kinetics−Two or more conc. of hot." equation (GraphPad Prism software) was fitted to the data points (R^2 = 0.83). (F) Monitoring the dissociation kinetics of compound **33**. Compound **33** was displaced from the receptor by the application of 100 μM atropine. The "One phase decay" equation was fitted to the data points (R^2 = 0.88). Data in (A), (B), (D), and (F) are presented as the mean ± SD of three independent biological replicates.

absorbance, excitation, and emission maxima show no significant change in PBS with and without BSA, as shown in Figure S1. Finally, to prove the ability for biological application, we have investigated the photostability of **33** in PBS (pH 7) excited with UV light (4 W, 450 nm). Half of the original fluorescence intensity was reached after 10 min of irradiation, which is still considered appropriate because a typical imaging process does not require longer continuous excitation.[20]

The M_1R−M_5R affinities of the intermediates **28**, **30**, **32** and the fluorescently labeled derivative **33** were determined at membranes from CHO cells transfected with hM_xR (x = 1−5) using the orthosteric antagonist [^{3}H]-scopolamine (*N*-methyl) as a radioligand (for competition binding curves, see Figure S2). Before testing the fluorescent probe (**33**), we checked for the binding affinity and selectivity of the base derivative (**28**) and the PEG linker-containing derivatives (**30**, **32**). The corresponding K_i values are listed in Table 1.

We observed that the initial molecule (**28**) exhibited lower selectivity for the M_4 receptor than previously reported in the literature.[9] This discrepancy is likely due to differences in the assay conditions used during our testing.

Interestingly, the application of the dye enhances the selectivity of the molecule across all four additional receptors (M_1, M_{3-5}). The new fluorescent ligand **33** we developed is a more selective M_2R probe compared to the dibenzodiazepinone-type fluorescent compounds reported in the literature.[20,17] Its selectivity for the M_1 and M_3 receptors is particularly notable, while its selectivity for the M_4 and M_5 receptors is comparable to those of previously published compounds (see Figure 2).

The ability of the compounds to antagonize the carbachol-induced G protein activation of M_2R was assessed using the bioluminescence resonance energy transfer (BRET)-based TRUPATH G_{oA} activation assay (Figure 4A,B).[37] All synthesized compounds (**28**, **30**, **32**, and **33**) acted as

https://doi.org/10.1021/acsmedchemlett.4c00592
ACS Med. Chem. Lett. 2025, 16, 552−559

competitive antagonists, displaying similar half-inhibitory concentration (IC_{50}) values (Table 2).

Table 2. IC_{50} Values for Carbachol-Induced G_{oA} Protein Activation[a]

Compound	Log(IC_{50}) ± SD (M)
28	−7.10 ± 0.23
30	−6.88 ± 0.13
32	−6.97 ± 0.12
33	−7.39 ± 0.09

[a]TRUPATH GoA biosensor-expressing HEK 293T cells were treated with the indicated compounds at increasing concentrations for 20 min, followed by stimulation with 10 μM carbachol for 15 min, as shown in Figure 4A,B. Concentration−response curves were fitted with GraphPad Prism 9 software (Hill-slope = 1, n = 3).

The suitability of the fluorescent compound for BRET-based ligand binding measurements was also evaluated (Figure 4). In these experiments, binding of the fluorescent receptor ligand to the BRET donor-fused receptor construct ensures a molecular proximity, resulting in resonance energy transfer and an increase in the BRET ratio (Figure 4C).[38,39] The specificity of the signal can be verified by treatment with nonlabeled competitive receptor ligands, which prevents the BRET signal. To generate the BRET donor labeled receptor construct, we fused the bright *Gaussia* luciferase enzyme[39] to the N-terminus of M_2R. In our measurements, a concentration-dependent and specific increase in the BRET signal was observed after treatment with **33**, yielding a dissociation constant (K_D) of 119 nM (Figure 4D). This value is higher than the K_i value obtained from the radioligand binding assay, likely due to differences in the experimental conditions and the receptor constructs used. The amplitude of the specific BRET ratio change was relatively low, potentially reflecting a suboptimal orientation of the BRET partners, which may have limited the efficiency of the resonance energy transfer. However, the low variability in the signal ensured precise and reliable measurements. Competitive ligand binding measurements were performed using unlabeled M_2R ligands, specifically atropine and compound **28** (Figure S3). This assay also proved to be effective for determining kinetic ligand binding parameters (Figure 4E,F). The calculated association and dissociation rate constants were 8.06 × 10^{-3} s^{-1} M^{-1} and 8.67 × 10^{-4} s^{-1}, respectively.

Having validated **33** as a selective and useful fluorescent probe for M_2R pharmacological investigations, we next examined the potential for visualization of M_2R in live transfected HEK 293T cells by confocal microscopy. HEK 293T cells were transfected with Cerulean-labeled M_2 receptors, and nontransfected cells were used as controls. The images revealed significant labeling in M_2R−Cerulean-expressing cells (Figure 5A) after addition of **33**, whereas no labeling was observed in nontransfected cells (Figure 4B). The signal of **33** was not detected on the control cells during the examined time frame (3 min), but on the transfected cells, it remained unchanged. For additional confocal images, see Figures S4, S5, and S9. To evaluate the specificity of the binding, the receptors pretreated with atropine show no labeling with ligand **33**, as shown in Figure S6.

Confocal microscopy results confirmed the selective labeling of **33** against M_2 receptors. Based on the encouraging results, we have evaluated its potential in two-photon and higher-resolution imaging techniques.

We examined live M_2R cells with two-photon microscopy as well (Figure 6). A labeling pattern similar to that observed in the confocal microscopy studies was identified. Figure 6A illustrates **33** labeling in HA−M_2R-transfected cells. The labeling can be observed selectively only at the plasma membrane of cells where the receptors can be found. Similarly to the confocal images, no dye labeling was detected inside the cells. Figure 6B presents a microscopic image of nontransfected cells, showing a minor degree of autofluorescence. When the probe was applied to these nontransfected cells, no receptor labeling was observed. This investigation confirmed the usefulness of the fluorescent probe in two-photon microscopy and demonstrated the labeling of the M_2 receptors in living cells. For additional two-photon images, see Figures S7 and S8.

As STED microscopy is used for the deeper investigation of cellular processes even at the subcellular level, we challenged

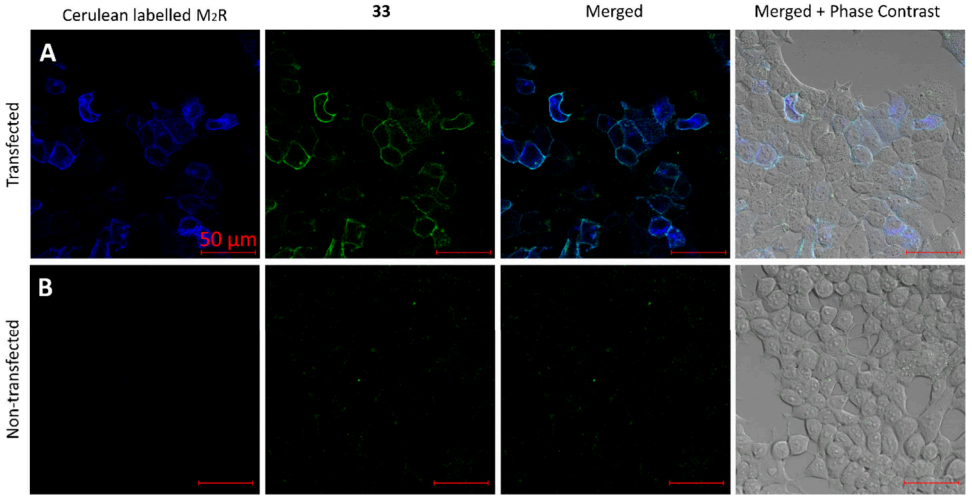

Figure 5. Visualization of **33** (300 nM) labeling of live M_2R−Cerulean-expressing HEK 293T cells using confocal microscopy. (A, B) Images obtained after 3 min from M_2R−Cerulean-transfected (A) and nontransfected (B) cells treated with **33** (300 nM). Blue represents the Cerulean fluorescence, and the fluorescent signal of **33** is shown in green. Scale bars: 50 μm. Representative images of two independent experiments are shown.

https://doi.org/10.1021/acsmedchemlett.4c00592
ACS Med. Chem. Lett. 2025, 16, 552−559

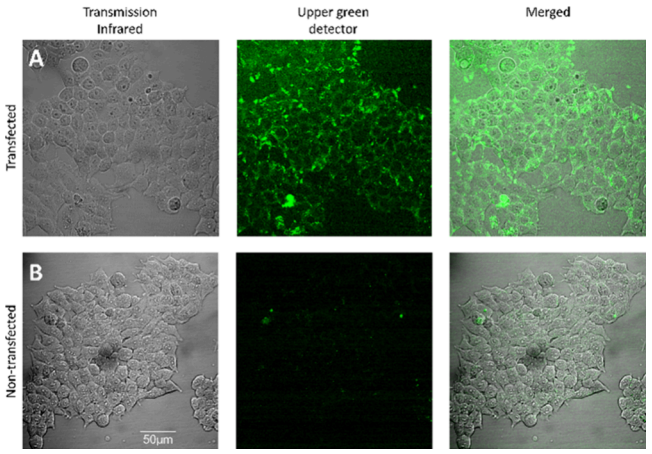

Figure 6. Two-photon microscopy imaging of M_2R using **33**. (A) **33** (300 nM) labeling of live HA−M_2R-transfected HEK 293T cells excited at 820 nm. (B) Images obtained from nontransfected HEK 293T cells. The green outlines show that **33** bound to the M_2 receptor in the plasma membrane. Scale bar: 50 μm. Representative images of two independent experiments are shown.

the fluorescent probe **33** in STED nanoscopy (Figure 7). For STED, we used the same transfected cells as in the case of two-photon microscopy. Using the STED function and the available largest magnification objective, we observed improvement of optical resolution. The **33** green signal is concentrated in the membranes of cells, where the M_2Rs are located.

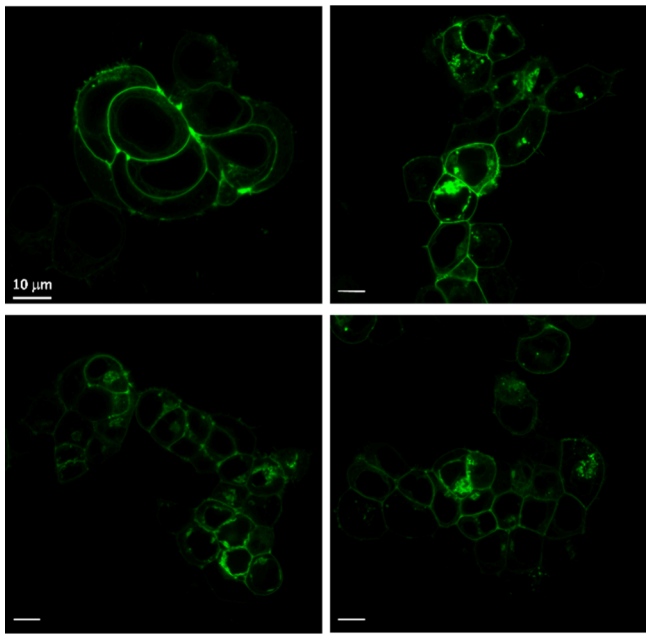

Figure 7. Images with the STED function of living cells expressing HA−M_2R stained with **33**. The green color represents **33** (300 nM) labeling. Scale bar: 10 μm. Representative images of two independent experiments are shown. For control STED images, see Figure S10.

In conclusion, the diverse functions and structural characteristics of the M_2 receptor make it a critical target for understanding its role under various physiological and pathological conditions. Extending the possibilities of molecular level investigations, we have developed a new anthranilamide-based fluorescent probe for M_2R. The conjugate has a nanomolar affinity toward M_2R (K_i = 2.4 nM) and demonstrates greater selectivity compared to the previously reported dibenzodiazepinone derivatives. The OG488-labeled probe (**33**) exhibits suitable photophysical properties (λ_{abs}^{max}: 520, λ_{max}^{em}: 547, ε: 42504.9 M^{-1} cm^{-1}, Φ_f: 0.20), making it highly suitable for microscopy. In order to demonstrate its versatility, we successfully applied it in confocal microscopy, two-photon microscopy imaging, and STED imaging with living cells. Due to the selected Oregon Green 488 dye, the ideal kinetic properties, and beneficial selectivity profile, the probe has the potential to unlock new avenues for investigating M_2R trafficking, interactions, and its involvement in diverse signaling pathways at high resolution with a broad range of microscopic methods.

■ ASSOCIATED CONTENT

Supporting Information

The Supporting Information is available free of charge at https://pubs.acs.org/doi/10.1021/acsmedchemlett.4c00592.

General chemistry methods; computational modeling; photophysical measurements; radioligand competition binding studies; in vitro pharmacology; microscopy imaging; synthetic procedures; ^{1}H and ^{13}C NMR spectra (PDF)

■ AUTHOR INFORMATION

Corresponding Author

György Miklós Keserű − *Medicinal Chemistry Research Group, HUN-REN Research Centre for Natural Sciences, H-1117 Budapest, Hungary; Department of Organic Chemistry and Technology, Budapest University of Technology and Economics, H-1111 Budapest, Hungary; National Laboratory for Drug Research and Development, H-1117 Budapest, Hungary;* orcid.org/0000-0003-1039-7809; Email: keseru.gyorgy@ttk.hu

Authors

Renáta Szabó − *Medicinal Chemistry Research Group, HUN-REN Research Centre for Natural Sciences, H-1117 Budapest, Hungary; Department of Organic Chemistry and Technology, Budapest University of Technology and Economics, H-1111 Budapest, Hungary; National Laboratory for Drug Research and Development, H-1117 Budapest, Hungary*

Dénes Szepesi Kovács − *Medicinal Chemistry Research Group, HUN-REN Research Centre for Natural Sciences, H-1117 Budapest, Hungary; Department of Organic Chemistry and Technology, Budapest University of Technology and Economics, H-1111 Budapest, Hungary; National Laboratory for Drug Research and Development, H-1117 Budapest, Hungary*

Dóra Judit Kiss − *Medicinal Chemistry Research Group, HUN-REN Research Centre for Natural Sciences, H-1117 Budapest, Hungary; National Laboratory for Drug Research and Development, H-1117 Budapest, Hungary*

Zeinab Nezafat Yazdi − *Institute of Molecular Life Sciences, Centre of Excellence of the Hungarian Academy of Sciences, HUN-REN Research Centre for Natural Sciences, H-1117 Budapest, Hungary*

András Dávid Tóth − *Institute of Molecular Life Sciences, Centre of Excellence of the Hungarian Academy of Sciences, HUN-REN Research Centre for Natural Sciences, H-1117*

Budapest, Hungary; Department of Internal Medicine and Haematology, Semmelweis University, H-1088 Budapest, Hungary

Jose Brea − *Innopharma Drug Screening and Pharmacogenomics Platform, BioFarma Research Group, Center for Research in Molecular Medicine and Chronic Diseases (CiMUS), Department of Pharmacology, Pharmacy, and Pharmaceutical Technology, University of Santiago de Compostela, 15705 Santiago de Compostela, Spain*

María Isabel Loza − *Innopharma Drug Screening and Pharmacogenomics Platform, BioFarma Research Group, Center for Research in Molecular Medicine and Chronic Diseases (CiMUS), Department of Pharmacology, Pharmacy, and Pharmaceutical Technology, University of Santiago de Compostela, 15705 Santiago de Compostela, Spain;* orcid.org/0000-0003-4730-0863

Domokos Mészéna − *Department of Neurology, Center for Neurotechnology and Neurorecovery, Massachusetts General Hospital, Harvard Medical School, Boston, Massachusetts 02114, United States; Integrative Neuroscience Research Group, Institute of Cognitive Neuroscience and Psychology, HUN-REN Research Centre for Natural Sciences, H-1117 Budapest, Hungary;* orcid.org/0000-0003-4042-2542

Lucia Wittner − *National Laboratory for Drug Research and Development, H-1117 Budapest, Hungary; Integrative Neuroscience Research Group, Institute of Cognitive Neuroscience and Psychology, HUN-REN Research Centre for Natural Sciences, H-1117 Budapest, Hungary*

István Ulbert − *National Laboratory for Drug Research and Development, H-1117 Budapest, Hungary; Integrative Neuroscience Research Group, Institute of Cognitive Neuroscience and Psychology, HUN-REN Research Centre for Natural Sciences, H-1117 Budapest, Hungary; Department of Neurosurgery and Neurointervention, Semmelweis University, H-1145 Budapest, Hungary; Department of Information Technology and Bionics, Péter Pázmány Catholic University, H-1083 Budapest, Hungary*

Balázs Volk − *Directorate of Drug Substance Development, Egis Pharmaceuticals Plc., H-1475 Budapest, Hungary;* orcid.org/0000-0002-2019-1874

László Hunyady − *Institute of Molecular Life Sciences, Centre of Excellence of the Hungarian Academy of Sciences, HUN-REN Research Centre for Natural Sciences, H-1117 Budapest, Hungary; Department of Physiology, Faculty of Medicine, Semmelweis University, H-1094 Budapest, Hungary*

Complete contact information is available at: https://pubs.acs.org/10.1021/acsmedchemlett.4c00592

Notes

The authors declare no competing financial interest.

■ ACKNOWLEDGMENTS

This work was supported by the following institutions/grants: National Office of Research, Development and Innovation (PharmaLab, RRF-2.3.1-21-2022-00015, 2020-1.1.2-PIACI-KFI-2020-00039, and K 139231, OTKA Hungarian postdoctoral grant PD143582), the Hungarian Academy of Sciences (NAP2022-I-2/2022 NAP 3.0), the Hungarian National Research, Development and Innovation Fund (NKFIH K137886), the Hungarian National Brain Research Program 2017-1.2.1-NKP-2017 00002, 3.0, and the FLAG-ERA Joint Transnational Call 2021, VIPattract grant and Xunta de Galicia (ED431C 2022/20), and European Regional Development Fund (EDRF). Project C2246513, KDP-IKT-2023-900-I1-00000957/0000003 has been implemented with the support provided by the Ministry of Culture and Innovation of Hungary from the National Research, Development and Innovation fund, financed under the KDP-2023 funding scheme. We thank József Simon for HRMS measurements as well as Krisztina Balázs for her contributions to the synthetic work. We thank Attila Lehotzky for his assistance with the BRET measurements.

■ ABBREVIATIONS

M_2R, M_2 muscarinic acetylcholine receptor; GPCRs, G protein-coupled receptors; STED, stimulated emission depletion nanoscopy; mAChRs, muscarinic acetylcholine receptors; Ach, acetylcholine; AD, Alzheimer's disease; OG488, Oregon Green 488; IFD, induced fit docking; PEG, polyethylene glycol; PBS, phosphate buffered saline; BRET, bioluminescence resonance energy transfer; CHO, Chinese hamster ovary; HEK, human embryonic kidney; NMR, nuclear magnetic resonance; HRMS, high-resolution mass spectrometry

■ REFERENCES

(1) Hulme, E. C. Muscarinic Receptor Subtypes. *Annu. Rev. Pharmacol. Toxicol.* **1990**, *30*, 633−673.

(2) Brown, D. A. Muscarinic Acetylcholine Receptors (MAChRs) in the Nervous System: Some Functions and Mechanisms. *J. Mol. Neurosci.* **2010**, *41* (3), 340−346.

(3) Thomsen, M.; Sørensen, G.; Dencker, D. Physiological Roles of CNS Muscarinic Receptors Gained from Knockout Mice. *Neuropharmacology* **2018**, *136*, 411−420.

(4) Wess, J.; Eglen, R. M.; Gautam, D. Muscarinic Acetylcholine Receptors: Mutant Mice Provide New Insights for Drug Development. *Nat. Rev. Drug Discovery* **2007**, *6* (9), 721−733.

(5) Greenlee, W.; Clader, J.; Asberom, T.; McCombie, S.; Ford, J.; Guzik, H.; Kozlowski, J.; Li, S.; Liu, C.; Lowe, D.; Vice, S.; Zhao, H.; Zhou, G.; Billard, W.; Binch, H.; Crosby, R.; Duffy, R.; Lachowicz, J.; Coffin, V.; Watkins, R.; Ruperto, V.; Strader, C.; Taylor, L.; Cox, K. Muscarinic Agonists and Antagonists in the Treatment of Alzheimer's Disease. *Farmaco* **2001**, *56* (4), 247−250.

(6) Doods, H.; Entzeroth, M.; Ziegler, H.; Schiavi, G.; Engel, W.; Mihm, G.; Rudolf, K.; Eberlein, W. Characterization of BIBN 99: A Lipophilic and Selective Muscarinic M2 Receptor Antagonist. *Eur. J. Pharmacol.* **1993**, *242* (1), 23−30.

(7) Micheletti, R.; Montagna, E.; Giachetti, A. AF-DX 116, a Cardioselective Muscarinic Antagonist. *J. Pharmacol. Exp. Ther.* **1987**, *241* (2), 628−634.

(8) Francotte, P.; de Tullio, P.; Fraikin, P.; Pirotte, B. New Trends in the Design of Drugs Against Alzheimer's Disease. *Front. Med. Chem. - (Volume 3)* **2012**, 249−284.

(9) Clader, J. W.; Billard, W.; Binch, H.; Chen, L. Y.; Crosby, G.; Duffy, R. A.; Ford, J.; Kozlowski, J. A.; Lachowicz, J. E.; Li, S.; Liu, C.; McCombie, S. W.; Vice, S.; Zhou, G.; Greenlee, W. J. Muscarinic M2 Antagonists: Anthranilamide Derivatives with Exceptional Selectivity and in Vivo Activity. *Bioorg. Med. Chem.* **2004**, *12* (2), 319−326.

(10) Tahtaoui, C.; Parrot, I.; Klotz, P.; Guillier, F.; Galzi, J. L.; Hibert, M.; Ilien, B. Fluorescent Pirenzepine Derivatives as Potential Bitopic Ligands of the Human M1Muscarinic Receptor. *J. Med. Chem.* **2004**, *47* (17), 4300−4315.

(11) Daval, S. B.; Kellenberger, E.; Bonnet, D.; Utard, V.; Galzi, J. L.; Ilien, B. Exploration of the Orthosteric/Allosteric Interface in Human M1Muscarinic Receptors by Bitopic Fluorescent Ligandss. *Mol. Pharmacol.* **2013**, *84* (1), 71−85.

(12) Jacobson, K. A.; Fischer, B.; van Rhee, A.M. Molecular Probes for Muscarinic Receptors: Functionalized Congeners of Selective Muscarinic Antagonists. *Life Sci.* **1995**, *56*, 823−830.
(13) Hern, J. A.; Baig, A. H.; Mashanov, G. I.; Birdsall, B.; Corrie, J. E. T.; Lazareno, S.; Molloy, J. E.; Birdsall, N. J. M. Formation and Dissociation of M1Muscarinic Receptor Dimers Seen by Total Internal Reflection Fluorescence Imaging of Single Molecules. *Proc. Natl. Acad. Sci. U. S. A.* **2010**, *107* (6), 2693−2698.
(14) Harris, A.; Cox, S.; Burns, D.; Norey, C. Miniaturization of Fluorescence Polarization Receptor-Binding Assays Using CyDye-Labeled Ligands. *J. Biomol. Screen.* **2003**, *8* (4), 410−420.
(15) Daval, S. B.; Valant, C.; Bonnet, D.; Kellenberger, E.; Hibert, M.; Galzi, J. L.; Ilien, B. Fluorescent Derivatives of AC-42 to Probe Bitopic Orthosteric/Allosteric Binding Mechanisms on Muscarinic M1 Receptors. *J. Med. Chem.* **2012**, *55* (5), 2125−2143.
(16) Jones, L. H.; Randall, A.; Napier, C.; Trevethick, M.; Sreckovic, S.; Watson, J. Design and Synthesis of a Fluorescent Muscarinic Antagonist. *Bioorg. Med. Chem. Lett.* **2008**, *18* (2), 825−827.
(17) Gruber, C. G.; Pegoli, A.; Müller, C.; Grätz, L.; She, X.; Keller, M. Differently Fluorescence-Labelled Dibenzodiazepinone-Type Muscarinic Acetylcholine Receptor Ligands with High M2R Affinity. *RSC Med. Chem.* **2020**, *11* (7), 823−832.
(18) Keller, M.; Tränkle, C.; She, X.; Pegoli, A.; Bernhardt, G.; Buschauer, A.; Read, R. W. M2 Subtype Preferring Dibenzodiazepinone-Type Muscarinic Receptor Ligands: Effect of Chemical Homo-Dimerization on Orthosteric (and Allosteric?) Binding. *Bioorg. Med. Chem.* **2015**, *23* (14), 3970−3990.
(19) Pegoli, A.; She, X.; Wifling, D.; Hübner, H.; Bernhardt, G.; Gmeiner, P.; Keller, M. Radiolabeled Dibenzodiazepinone-Type Antagonists Give Evidence of Dualsteric Binding at the M2Muscarinic Acetylcholine Receptor. *J. Med. Chem.* **2017**, *60* (8), 3314−3334.
(20) She, X.; Pegoli, A.; Gruber, C. G.; Wifling, D.; Carpenter, J.; Hübner, H.; Chen, M.; Wan, J.; Bernhardt, G.; Gmeiner, P.; Holliday, N. D.; Keller, M. Red-Emitting Dibenzodiazepinone Derivatives as Fluorescent Dualsteric Probes for the Muscarinic Acetylcholine M2 Receptor. *J. Med. Chem.* **2020**, *63* (8), 4133−4154.
(21) Gitler, M. S.; Reba, R. C.; Cohen, V. I.; Rzeszotarski, W. J.; Baumgold, J. A Novel M2-Selective Muscarinic Antagonist: Binding Characteristics and Autoradiographic Distribution in Rat Brain. *Brain Res.* **1992**, *582* (2), 253−260.
(22) Jullié, D.; Valbret, Z.; Stoeber, M. Optical Tools to Study the Subcellular Organization of GPCR Neuromodulation. *J. Neurosci. Methods* **2022**, *366*, 109408.
(23) Stoddart, L. A.; Kindon, N. D.; Otun, O.; Harwood, C. R.; Patera, F.; Veprintsev, D. B.; Woolard, J.; Briddon, S. J.; Franks, H. A.; Hill, S. J.; Kellam, B. Ligand-Directed Covalent Labelling of a GPCR with a Fluorescent Tag in Live Cells. *Commun. Biol.* **2020**, *3* (1), 1−9.
(24) Dekkers, S.; Caspar, B.; Goulding, J.; Kindon, N. D.; Kilpatrick, L. E.; Stoddart, L. A.; Briddon, S. J.; Kellam, B.; Hill, S. J.; Stocks, M. J. Small-Molecule Fluorescent Ligands for the CXCR4 Chemokine Receptor. *J. Med. Chem.* **2023**, *66* (7), 5208−5222.
(25) Comeo, E.; Kindon, N. D.; Soave, M.; Stoddart, L. A.; Kilpatrick, L. E.; Scammells, P. J.; Hill, S. J.; Kellam, B. Subtype-Selective Fluorescent Ligands as Pharmacological Research Tools for the Human Adenosine A2A Receptor. *J. Med. Chem.* **2020**, *63* (5), 2656−2672.
(26) Rosier, N.; Grätz, L.; Schihada, H.; Möller, J.; Işbilir, A.; Humphrys, L. J.; Nagl, M.; Seibel, U.; Lohse, M. J.; Pockes, S. A Versatile Sub-Nanomolar Fluorescent Ligand Enables NanoBRET Binding Studies and Single-Molecule Microscopy at the Histamine H3Receptor. *J. Med. Chem.* **2021**, *64* (15), 11695−11708.
(27) Nagl, M.; Mönnich, D.; Rosier, N.; Schihada, H.; Sirbu, A.; Konar, N.; Reyes-Resina, I.; Navarro, G.; Franco, R.; Kolb, P.; Annibale, P.; Pockes, S. Fluorescent Tools for the Imaging of Dopamine D2-Like Receptors**. *ChemBioChem.* **2024**, *25* (2), No. e202300659.
(28) Cai, M.; Stankova, M.; Pond, S. J. K.; Mayorov, A. V.; Perry, J. W.; Yamamura, H. I.; Trivedi, D.; Hruby, V. J. Real Time Differentiation of G-Protein Coupled Receptor (GPCR) Agonist and Antagonist by Two Photon Fluorescence Laser Microscopy. *J. Am. Chem. Soc.* **2004**, *126* (23), 7160−7161.
(29) Szepesi Kovács, D.; Chiovini, B.; Müller, D.; Tóth, E. Z.; Fülöp, A.; Ábrányi-Balogh, P.; Wittner, L.; Várady, G.; Farkas, Ö.; Turczel, G.; Katona, G.; Győrffy, B.; Keserű, G. M.; Mucsi, Z.; Rózsa, B. J.; Kovács, E. Synthesis and Application of Two-Photon Active Fluorescent Rhodol Dyes for Antibody Conjugation and In Vitro Cell Imaging. *ACS Omega* **2023**, *8* (25), 22836−22843.
(30) Butkevich, A. N.; Mitronova, G. Y.; Sidenstein, S. C.; Klocke, J. L.; Kamin, D.; Meineke, D. N. H.; D'Este, E.; Kraemer, P. T.; Danzl, J. G.; Belov, V. N.; Hell, S. W. Fluorescent Rhodamines and Fluorogenic Carbopyronines for Super-Resolution STED Microscopy in Living Cells. *Angew. Chemie - Int. Ed.* **2016**, *55* (10), 3290−3294.
(31) Mitronova, G. Y.; Lukinavičius, G.; Butkevich, A. N.; Kohl, T.; Belov, V. N.; Lehnart, S. E.; Hell, S. W. High-Affinity Functional Fluorescent Ligands for Human β-Adrenoceptors. *Sci. Rep.* **2017**, *7* (1), 1−15.
(32) Jeong, S.; Widengren, J.; Lee, J. C. Fluorescent Probes for Sted Optical Nanoscopy. *Nanomaterials* **2022**, *12* (1), 21.
(33) Suno, R.; Lee, S.; Maeda, S.; Yasuda, S.; Yamashita, K.; Hirata, K.; Horita, S.; Tawaramoto, M. S.; Tsujimoto, H.; Murata, T.; Kinoshita, M.; Yamamoto, M.; Kobilka, B. K.; Vaidehi, N.; Iwata, S.; Kobayashi, T. Structural Insights into the Subtype-Selective Antagonist Binding to the M2Muscarinic Receptor. *Nat. Chem. Biol.* **2018**, *14* (12), 1150−1158.
(34) Suzuki, T.; Hisakawa, S.; Itoh, Y.; Suzuki, N.; Takahashi, K.; Kawahata, M.; Yamaguchi, K.; Nakagawa, H.; Miyata, N. Design, Synthesis, and Biological Activity of Folate Receptor-Targeted Prodrugs of Thiolate Histone Deacetylase Inhibitors. *Bioorg. Med. Chem. Lett.* **2007**, *17* (15), 4208−4212.
(35) Zeng, L.; Fu, H.; Qiao, R.; Jiang, Y.; Zhao, Y. Efficient Copper-Catalyzed Synthesis of N-Alkylanthranilic Acids via an Ortho-Substituent Effect of the Carboxyl Group of 2-Halobenzoic Acids at Room Temperature. *Adv. Synth. Catal.* **2009**, *351* (10), 1671−1676.
(36) Sun, W. C.; Gee, K. R.; Klaubert, D. H.; Haugland, R. P. Synthesis of Fluorinated Fluoresceins. *J. Org. Chem.* **1997**, *62* (19), 6469−6475.
(37) Kroeze, W. K.; Sassano, M. F.; Huang, X. P.; Lansu, K.; McCorvy, J. D.; Giguère, P. M.; Sciaky, N.; Roth, B. L. PRESTO-Tango as an Open-Source Resource for Interrogation of the Druggable Human GPCRome. *Nat. Struct. Mol. Biol.* **2015**, *22* (5), 362−369.
(38) Stoddart, L. A.; Johnstone, E. K. M.; Wheal, A. J.; Goulding, J.; Robers, M. B.; MacHleidt, T.; Wood, K. V.; Hill, S. J.; Pfleger, K. D. G. Application of BRET to Monitor Ligand Binding to GPCRs. *Nat. Methods* **2015**, *12* (7), 661−663.
(39) Tóth, A. D.; Garger, D.; Prokop, S.; Soltész-Katona, E.; Várnai, P.; Balla, A.; Turu, G.; Hunyady, L. A General Method for Quantifying Ligand Binding to Unmodified Receptors Using Gaussia Luciferase. *J. Biol. Chem.* **2021**, *296*, 100366.

https://doi.org/10.1021/acsmedchemlett.4c00592
ACS Med. Chem. Lett. 2025, 16, 552−559